Solar control of radar wave absorption by the Martian ionosphere

D. D. Morgan,[1] D. A. Gurnett,[1] D. L. Kirchner,[1] R. L. Huff,[1] D. A. Brain,[2] W. V. Boynton,[3] M. H. Acuña,[4] J. J. Plaut,[5] and G. Picardi[6]

Received 19 April 2006; revised 24 May 2006; accepted 7 June 2006; published 13 July 2006.

[1] The MARSIS active sounder aboard the Mars Express spacecraft, under certain conditions in the Martian ionosphere, fails to detect the planetary surface. We have generated a statistical measure of the surface reflection visibility, which we plot as a time series and compare with both in situ particle data taken at Mars and solar x-ray data taken at Earth. We show that loss of the surface signal is closely related to the influx of solar protons at tens of MeV energies. We infer that the influx of high energy solar protons causes impact ionization, increasing the electron density in the Martian ionosphere. At altitudes close to or below 100 km, where the electron-neutral collision frequency is high and the electron density typically has a local maximum, the increased electron density raises the damping coefficient to levels sufficient for complete absorption of the sounding wave over an altitude range of a few tens of kilometers. **Citation:** Morgan, D. D., D. A. Gurnett, D. L. Kirchner, R. L. Huff, D. A. Brain, W. V. Boynton, M. H. Acuña, J. J. Plaut, and G. Picardi (2006), Solar control of radar wave absorption by the Martian ionosphere, *Geophys. Res. Lett.*, *33*, L13202, doi:10.1029/2006GL026637.

1. Introduction

[2] Mars Express, which was launched on June 2 and put in orbit about Mars on December 25, 2003, carries a radar sounding experiment named MARSIS (Mars Advanced Radar for Subsurface and Ionospheric Sounding) [*Chicarro et al.*, 2004; *Picardi et al.*, 2004], which comprises several modes designed to probe the ionosphere, the surface, and subsurface regions of Mars. The Active Ionospheric Sounder (AIS) mode is designed to probe the Martian ionosphere but also detects the surface of the planet. We have seen that for periods of days or weeks, following episodes of solar flare activity, the surface reflection may disappear altogether. This interesting ionospheric phenomenon has implications for surface and subsurface science at Mars, because when MARSIS AIS cannot detect the surface, output of the MARSIS subsurface radar mode is severely degraded. Thus it is of general interest to investigate the mechanism that causes radio wave absorption. In this paper we will discuss the circumstances under which ionospheric absorption of low frequency radio waves occurs.

[3] An example of a solar flare affecting the Martian ionosphere is shown in Figure 3b of *Gurnett et al.* [2005], in which a large excursion from expected maximum electron density is detected by MARSIS coincident with a class X1.1 flare on September 15, 2005. This event, which lasted about ten minutes, was almost certainly caused by the x-ray and XUV radiation associated with the flare, analogous to a Sudden Ionospheric Disturbance (SID) at Earth [see *Mitra*, 1974]. *Mendillo et al.* [2006] discuss similar events detected by the Mars Global Surveyor spacecraft on April 15, 16 and 26, 2001. Although the radio occultation technique does not determine the time length of an event, we expect, because of the recombination time on the order of seconds, that these events will be short-lived, on a time scale comparable to the duration of the x-ray or XUV enhancement marking the flare. This mechanism, while effective at increasing the peak plasma frequency, cannot explain the extended periods of loss of the surface reflection that are observed and that impede the use of the subsurface sounder.

[4] Luckily, an analogous case of absorption occurs at Earth. Absorption of the cosmic radio background has long been observed over the Earth's polar caps. The occurrence of polar cap absorption events (PCAs [*Bailey*, 1964]) in the polar caps and only during solar disturbances indicates that PCAs are caused by charged particles originating at the sun. *Patterson et al.* [2001] found the mechanism for absorption to be impact ionization due to an influx of solar energetic protons, leading to increased electron density. The increased electrons in turn cause an increase in electron-neutral collision damping of radio waves. Patterson et al. used riometer data from the Antarctic in conjunction with data from the Charged Particle Measurement Experiment aboard the IMP-8 spacecraft to show that 20 MeV protons are most efficient at generating the needed ionization.

[5] In this paper, we shall compare the occurrence of sounding wave absorption events detected by MARSIS with available particle and x-ray data to see if this model is applicable at Mars.

2. Theory

[6] We believe that sounding wave absorption is controlled by an influx of solar energetic protons, similar to the PCAs discussed by *Patterson et al.* [2001]. According to this model, the incoming particles ionize a population of neutrals at altitudes lower than normal for photoionization. An impinging radio wave then includes the excess electrons in its wave motion, increasing collisions with neutrals. At altitudes where the electron-neutral collision frequency is high, the collisions convert wave energy into thermal energy

[1]Department of Physics and Astronomy, University of Iowa, Iowa City, Iowa, USA.
[2]Space Physics Research Group, Space Sciences Laboratory, University of California, Berkeley, California, USA.
[3]Lunar and Planetary Laboratory, University of Arizona, Tucson, Arizona, USA.
[4]NASA Goddard Space Flight Center, Greenbelt, Maryland, USA.
[5]Jet Propulsion Laboratory, Pasadena, California, USA.
[6]Infocom Department, "La Sapienza", University of Rome, Rome, Italy.

0094-8276/06/2006GL026637$05.00

of neutral particles at a rate high enough to completely damp the wave.

[7] The dispersion relation for an electromagnetic wave with collision damping in the absence of a magnetic field is given by [e.g., *Budden*, 1961, p. 40]

$$k = \frac{\omega}{c}\sqrt{1 - \left(\frac{\omega_{pe}}{\omega}\right)^2 \Big/ \left(1 - i\frac{\nu_{e,n}}{\omega}\right)} \tag{1}$$

where k is the wave number, ω the sounding wave angular frequency, ω_{pe} the plasma angular frequency, $\nu_{e,n}$ the electron-neutral collision frequency, and c the vacuum speed of light = 3×10^5 km/s.

[8] When $\nu_{e,n}/\omega$ becomes negligible, equation (1) becomes

$$k = \frac{\omega}{c}\sqrt{1 - \left(\frac{\omega_{pe}}{\omega}\right)^2} \tag{2}$$

whence the phase velocity is

$$v_{phase} = \frac{c}{\sqrt{1 - \left(\omega_{pe}/\omega\right)^2}} \tag{3}$$

and the group velocity is

$$v_{group} = c\sqrt{1 - \left(\omega_{pe}/\omega\right)^2} \tag{4}$$

When $\nu_{e,n}/\omega \ll 1$, the damping wave number is given by

$$k_i \simeq \left(\frac{\nu_{e,n}}{2c}\right)\frac{\omega_{pe}^2}{\omega^2\sqrt{\left(1 - \left(\omega_{pe}/\omega\right)^2\right)}} \tag{5}$$

which, when $\omega \gg \omega_{pe}$, becomes [*Gurnett and Bhattacharjee*, 2005, p. 132]

$$k_i \simeq -\frac{\nu_{e,n}\omega_{pe}^2}{2c\omega^2} \tag{6}$$

The electron-neutral collision frequency $\nu_{e,n}$ is given by [*Gurnett and Bhattacharjee*, 2005, p. 13]

$$\nu_{e,n} = n_n C_e \sigma_{e,n} \tag{7}$$

where n_n is the neutral particle density, C_e is the electron thermal speed, and $\sigma_{e,n}$ is the electron-neutral collision cross section. At Mars, the primary neutral species is CO_2. We use an empirical expression for the electron-CO_2 collision cross section, given by *Strangeway* [1996] as

$$\sigma_{e,CO_2}(cm^2) = 1.55 \times 10^{-15} + 2.76 \times 10^{-15} \cdot \exp[-11.88T_e(eV)]/[T_e(eV)]^{1/2} \tag{8}$$

We expect absorption to take place on the bottom side of the ionosphere around 100 km altitude. Ionospheric modeling by *Krasnopolsky* [2002] shows a maximum value of the electron density over the whole ionosphere at about 130 km altitude and a smaller bump at 100 km altitude. Taking values of T_e, n_e, and n_{CO2}, at these altitudes from his model and maximum frequency 5.5 MHz of the MARSIS active sounder, we estimate a maximum value for the damping coefficient of about 2×10^{-3}/km, at 130 km and 0.06/km at 100 km altitude. Because of the layered structure of the ionosphere, the damping must take place within a range of a few tens of kilometers, so the damping coefficient must approach 0.1/km. Krasnopolsky's model implies a damping coefficient at 100 km altitude that hovers just below that necessary for damping. Since this model is computed for a solar zenith angle of 60°, where surface reflection visibility varies considerably, this result is consistent with our hypothesis.

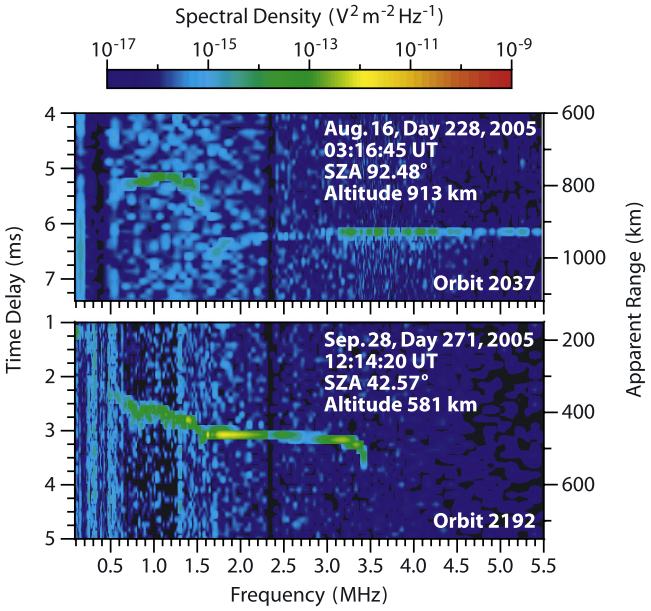

Figure 1. Each panel shows part of an ionogram, the principal form of graphic data output from the MARSIS active sounder. An ionogram shows the color-mapped intensity of the return signal as a function of frequency (horizontal axis) and time interval from emission of the sounding pulse, also known as the "delay time" (vertical axis). The apparent range is shown on the right side vertical axis. (top) An ionospheric reflection between frequencies of 0.5 and 1.5 MHz and 5 and 6s delay time, corresponding to between 700 and 900 km apparent range. At frequencies greater than 1.5 MHz, the apparent range of the reflected signal gradually approaches the spacecraft altitude, as one expects of the surface reflection. (bottom) An ionospheric reflection between 0.5 and 3.5 MHz and 2 and 4 ms delay time but no surface reflection.

[9] Recent results of *Pätzold et al.* [2005, 2006] have identified a sporadic ionospheric layer between 60 and 100 km altitude, which they designate the M3 layer. Whether the M3 layer could be the site of radio wave absorption is an open question.

3. Data

[10] Figure 1 shows two examples of ionograms, the principle form of graphic output from MARSIS AIS. This

data format consists of a map of reflected electromagnetic intensity as a function of the frequency of the sounding wave, displayed as the abscissa, and the "time delay," or, time interval from launch of the wave pulse to detection, displayed as the ordinate. An increase in intensity above background indicates the presence of a reflecting barrier. Any abrupt boundary in dielectric coefficient can cause this, in particular the surface of the planet or the plasma frequency becoming equal to the wave frequency [see equation (2)]. The apparent range, defined as the range inferred assuming that $V_g = c$ and given by

$$r_{apparent} = c\Delta t_{delay}/2 \tag{9}$$

is given as an equivalent ordinate on the right. In accord with equation (4), it is a good estimate of the actual range only if $\omega/\omega_{pe} \ll 1$ over the entire ray path.

[11] Figure 1 (top) shows the ionospheric reflection between frequencies of 0.5 and 5.5 MHz and delay times of 5 and 6 ms. There is then a jump in delay time to 6.7 ms, where the apparent range goes through an abrupt maximum (referred to as the cusp) followed by a gradual decrease, approaching the spacecraft altitude. The asymptotic approach of apparent range to spacecraft altitude with increasing frequency is characteristic of the surface reflection, because, as the frequency becomes much greater than the maximum plasma frequency, the group velocity of the sounding wave at all points on its path approaches the vacuum speed of light [see equation (4)]. This diagnostic makes it easy to determine whether one is seeing the surface reflection. For comparison, the ionogram in the bottom plot shows an ionospheric reflection but no surface reflection. We have catalogued the surface reflection visibility (0 for not visible, 1 for visible) for each ionogram. We will use these data to create a time series for representing the visibility of the surface reflection for comparison with particle and x-ray data.

[12] *Gurnett et al.* [2005] give a complete description of phenomena observed in MARSIS AIS ionograms.

[13] The statistic that we refer to as the averaged surface reflection visibility is computed by averaging ten samples of the surface reflection visibility around 850 km altitude on the outbound leg of each orbit over a period of approximately 90 days. The ten samples typically result in an altitude range of approximately ±10 km. A constant altitude was chosen to eliminate variation with altitude. The sampling is restricted in time and to the outbound leg of the orbit to constrain the sampled solar zenith angles to be greater than 50°, where the surface reflection will be visible most of the time. Since there is one averaged value per orbit, the time resolution of this measurement is the orbital period of Mars Express, about 7.5 h.

[14] In Figure 2, we compare the surface reflection data with several other data sets. The abscissa of all plots is day of year 2005, displayed with the solar zenith angle where samples were taken. The first panel shows the averaged surface reflection visibility, as explained above. The second panel shows count rate data from the Electron Reflectometer aboard Mars Global Surveyor (MGS ER). These data are smoothed over two hours to remove the orbital variation. The MGS ER background is largely due to particles that can penetrate the instrument housing. The top three energy channels of MGS ER, designed to count electrons at 11.2, 14.3, and 18.2 keV, are used to measure background count rates, since these channels are normally very weakly populated. During solar energetic particle events this penetrating background is dominated by protons at energies of 10s of MeV or higher. The base count rate during quiet conditions is about 10 counts per second.

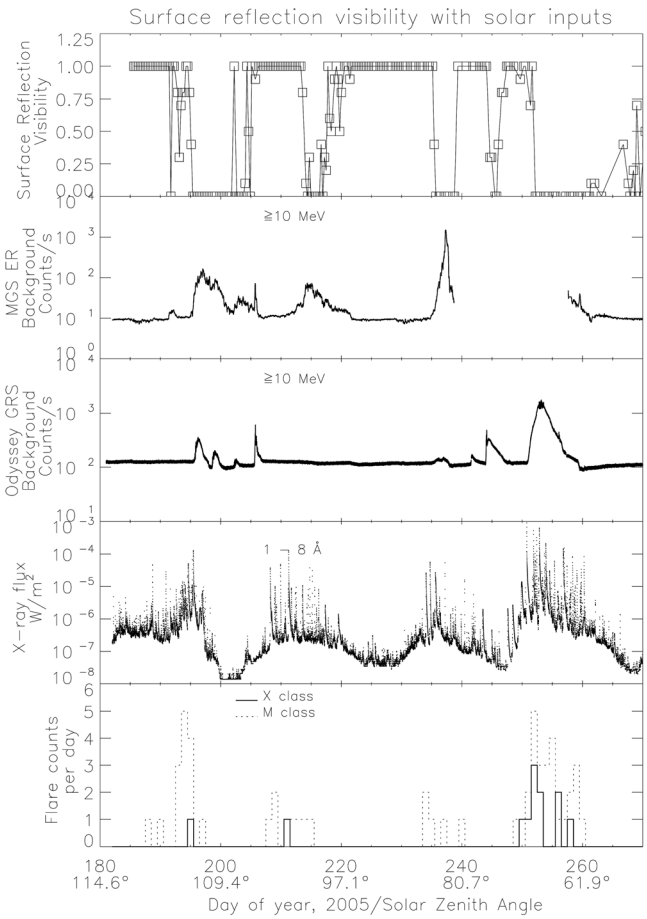

Figure 2. A time series plot comparing surface reflection visibility averaged over ten samples nearest 850 km altitude on the outbound leg of an orbit, with orbital period of 7.5 h (first panel). Also shown are Mars Global Surveyor Electron Reflectometer background (second panel), Mars Odyssey Gamma Ray Spectrometer (Upper Level Discriminator) background (third panel), soft x-ray emissions measured by the Solar Environment Monitor aboard GOES 12, with time adjusted for propagation to Mars (fourth panel), and NOAA daily flare counts (fifth panel). The abscissa of all plots is decimal day of year, 2005, accompanied by the solar zenith angle of the spacecraft where the samples shown in Figure 1 were taken. Periods where the surface reflection disappears are all clearly associated with particle enhancements, while four of the five events are associated with enhanced x-ray activity. Three of the five events are associated with X-class flares. Events 1 and 2 occur when the outbound leg of the Mars Express orbit is at solar zenith angles greater than 90°, i.e., the night side of Mars.

[15] The third panel shows count data from the Upper Level Discriminator of the Gamma Ray Spectrometer

Table 1. Times and SZAs of Absorption Events[a]

Event	Start Date-Time	End Date-Time	SZA, deg	Duration, d
1	07/10 (191) 09:31	07/25 (206) 08:33	113–106	15.0
2	08/01 (213) 06:47	08/09 (221) 17:12	102–96	8.4
3	08/23 (235) 03:10	08/27 (239) 07:51	85–81	4.2
4	09/01 (244) 02:23	09/04 (247) 11:12	77–74	3.4
5	09/05 (248) 13:53	09/23 (266) 18:16	73–55	18.2 ?

[a]Day of year 2005 is shown in parentheses.

aboard the Mars Odyssey spacecraft (Odyssey GRS). As in the second panel, the enhancements in background are due to penetrating radiation, largely protons at energy greater than 10 MeV. Unlike MGS ER, Odyssey GRS has a hard lower cutoff at 10 MeV. The base count rate is slightly above 100 counts per second.

[16] The fourth panel shows 1 – 8 Å x-ray flux from the Space Environment Monitor on GOES 12 in geosynchronous Earth orbit, and the fifth shows daily counts of X and M class solar flares, compiled by NOAA.

4. Observations

4.1. Overview of Observations

[17] The first panel of Figure 2 indicates that during the period under examination, July 1 through September 28, 2005, there were five major absorption events, when the surface reflection was lost for a significant period. We list these time intervals with their durations, in days, and range of solar zenith angle (SZA), in degrees, in Table 1. The orbital period of Mars Express is 7.5 h, which indicates that the uncertainty on the times listed is about 3.75 h or ±0.16 d. The second and third panels show at a glance that the five absorption intervals are associated with enhanced levels of solar energetic particles. The fourth panel shows that the absorption event onsets are usually associated with elevated x-ray fluxes but that the x-ray activity does not necessarily last for the duration of the event. The fifth panel shows that Events 1, 2, and 5 are associated with X-class (the highest energy class) flares, Event 3 is associated with M-class activity, and Event 4 is associated only with activity below M class. We note from the SZAs given with the abscissa that Events 1 and 2 are observed on the night side. The end of Event 5 is uncertain, because the SZA of the sampling is moving toward 50°, where the surface is often not visible.

4.2. Comparison and Discussion of Events

[18] In discussing the absorption events, all times will be given in decimal day of year, 2005.

4.2.1. Event 1

[19] During Event 1, the average surface reflection visibility decreases from a value of one a total of six times, at days 191.6, 192.6, 194.7, 202.5, 204.6, and 205.5. The first, third, fourth, and last of these intervals clearly coincide with enhancements in either or both of the particle instruments. X-rays, while active toward the start of the longest absorption interval, drop off to low levels at 196.8 and do not recover before the end of the event at 206.5. The absorption intervals starting at 192.6 and 204.6 have no obvious cause in either the particles or x-rays.

4.2.2. Event 2

[20] Event 2 features a deep onset at 213.5, followed by weak recovery and another onset at 214.9. The surface reflection disappears until 216.4, after which it recovers erratically until complete recovery at 221.6. These events are paralleled by particle enhancements in MGS ER from 212.4 to 213.6 and from 213.8 to 215.5, after which the particles decline slowly and erratically until they return to their base value at 221.7, nearly coinciding with the end of the absorption event. Odyssey GRS does not show an enhancement during this event.

[21] The x-rays show a major flare at 211.1, about 2 days before the main absorption onset. There are smaller x-ray events that occur closer to the absorption onset both prior to and throughout the period of absorption.

4.2.3. Event 3

[22] The averaged surface reflection visibility falls precipitously from one to zero at 235.3 and stays at zero until 238.8, returning to one at 239.3. This is accompanied by a steep rise and high maximum of the MGS ER background starting at 235.12 and a much smaller rise in the Odyssey GRS background starting at 235.1. The ER background drops sharply as the surface reflection reappears, but these data are unfortunately lost before they return to the base value. The GRS has returned to its base value by 238.0, somewhat before full recovery of the surface reflection.

[23] There are several M-class flares preceding and during Event 3, with x-ray spikes at 234.7, 235.7, 237.3, and a short-lived spike at 237.2. After 237.2, the x-rays are fairly quiet.

4.2.4. Event 4

[24] The onset of Event 4 corresponds with two closely spaced particle enhancements at 244.0 and 244.2, detected by Odyssey GRS. The GRS background hits its base level at 247.3, close to the end of the absorption event at 247.5. The onset of Event 4 corresponds only with flares of C class or lower and only with low x-ray fluxes. There is a low level x-ray enhancement at 243.5, preceding absorption onset at 244.4.

4.2.5. Event 5

[25] Event 5 has three onsets at 249.2, 251.0, and the deepest and longest lasting one, at 252.0. The surface reflection remains at zero until partial recovery at 261.4. A very high background enhancement in Odyssey GRS begins at day 251.1 and lasts until 259.4. We do not have MGS ER data through most of this event, but we can see its count rate tail off at 261.1.

[26] The principal onset of Event 5 coincides with a powerful solar flare at 251.9. Intense flare activity both precedes and coincides with the period of zero surface

reflection visibility. X-ray activity diminishes around 260.5, just before the start of recovery from absorption.

5. Interpretation and Conclusion

[27] Although each of the events we have identified is associated with both x-ray and particle activity, it is the particle activity that corresponds best with the timing of both onsets and recoveries. Furthermore, we observe the first two events at SZAs greater than 90°, implying that solar x-rays do not impinge directly on the atmosphere at the point of observation. In the case of Event 1, the absorption region at ~100 km is on the night side of Mars. This region is within reach of the sun during Event 2, but the radiation must penetrate the ionosphere from the side, which must severely reduce the solar intensity. On the other hand, as an approximate lower limit, the cyclotron radius of 10 MeV protons with 10° pitch angle in a magnetic field of 20 nT is on the order of the radius of Mars, implying that the energetic particles are much less severely shadowed than x-rays. The large cyclotron radius means that the electron density enhancements caused by solar proton events can be global in scale.

[28] We note that in Events 1 and 3, the surface reflection absorption continues for days after the x-rays have diminished. Event 4 is associated with only weak flares; however, its duration coincides well with the observed particle enhancement observed by Odyssey GRS. It is difficult to choose between particles and x-rays for Event 5, since both are very active for the duration of the event. On the whole we infer that it is the particle flux that controls the absorption of radio waves on time scales of days.

[29] Event 2 appears to be associated with an X-class flare, but, because the flare occurs about two days before the principal onset of absorption and protons at 10 MeV should typically take less than 2 h to get from the Sun to Mars, this appearance is deceptive. It is probable that these particles are associated with the lower-intensity flares occurring nearer the onset time of this event.

[30] The relation of solar activity to the absorption events we have recorded is complicated by the variation of the Earth–Sun–Mars angle between about 45° and 15° over the sampling interval of this study. It is possible that some events at Mars are associated with x-rays or flares not seen at Earth and that some x-ray and flare events detected at Earth are not effective at Mars. Active regions within the Earth–Sun–Mars angle of the limb of the Sun as seen from either planet (possibly adjusted for path of particle propagation) would fall into one of these categories. For example, examination of NOAA and NOAA/USAF archived solar activity data shows that the X-class flare preceding Event 2 occurs close to the dusk-side limb of the Sun as viewed from Mars, explaining its ineffectiveness in causing absorption.

[31] We note that, in Event 1, the principal absorption onset precedes the particle enhancement by 0.7 d. We suspect that the particles initiating this onset are low enough energy to be undetectable as background by either particle instrument. This same effect may explain the lack of a particle enhancement corresponding to two of the absorption intervals during Event 1. Enhancements of Odyssey GRS often lag behind those of MGS ER. We believe this is because the higher base count rate level of GRS means that it requires a higher count rate to make a detectable increase than for MGS ER.

[32] The region of absorption is not accessible to MARSIS AIS, since it must be below the electron density maximum at 130 km. The density layer around 100 km altitude, with a modest increase in electron density, could be the site of the observed absorption. Another possible absorption site is the sporadic M3 layer described by *Pätzold et al.* [2005, 2006].

[33] We conclude that surface reflection absorption events at Mars, lasting several days or longer, are best explained as resulting from an influx of solar energetic particles usually associated with solar x-ray flares. The absorption mechanism is that described by *Patterson et al.* [2001] in explaining PCAs. Protons at >10 MeV penetrate to altitudes of 100 km or lower, where they collisionally ionize the ambient atmospheric gas. The increased electron density in this region of high electron-neutral collision frequency causes an increase in the damping coefficient, as given in equation (6), signifying that radio wave energy is being converted to neutral kinetic energy through electron-neutral collisions. Because the ionization is triggered by charged particles moving helically along magnetic field lines, with cyclotron radius on the order of a Mars radius, the entire ionosphere of Mars is susceptible to radio wave absorption; we expect these events to be global in scale. This result is of intrinsic interest in the study of Mars; however, it is also useful to researchers using radar techniques to probe beneath the surface of Mars.

[34] **Acknowledgments.** We would like to thank Sharon Kutcher for her work in creating the surface reflection visibility data set and Edward West for writing the software tools used to display the ionograms. We acknowledge discussions with Paul Withers about the M3 ionospheric layer. This work was supported by NASA through contract 1224107 administered by the Jet Propulsion Laboratory.

References

Bailey, D. K. (1964), Polar-cap absorption, *Planet. Space Sci*, *12*, 495–541.

Budden, K. G. (1961), *Radio Waves in the Ionosphere*, Cambridge Univ. Press, New York.

Chicarro, A., P. Martin, and R. Traunter (2004), The Mars Express mission: An overview, in *Mars Express: A European Mission to the Red Planet*, *Eur. Space Agency Spec. Publ. SP-1240*, 3–16.

Gurnett, D. A., and A. Bhattacharjee (2005), *Introduction to Plasma Physics*, Cambridge Univ. Press, New York.

Gurnett, D. A., et al. (2005), The first radar soundings of the ionosphere of Mars, *Science*, *310*, 1929–1933.

Krasnopolsky, V. A. (2002), Mars' upper atmosphere and ionosphere at low, medium, and high solar activities: Implications for evolution of water, *J. Geophys. Res.*, *107*(E12), 5128, doi:10.1029/2001JE001809.

Mendillo, M., P. Withers, D. Hinson, H. Rishbeth, and B. Reinisch (2006), Effects of solar flares on the ionosphere of Mars, *Science*, *311*, 1135–1138.

Mitra, A. P. (1974), *Ionospheric Effects of Solar Flares*, Springer, New York.

Patterson, J. D., T. P. Armstrong, C. M. Laird, D. L. Derrick, and A. T. Weatherwax (2001), Correlation of solar energetic protons and polar cap absorption, *J. Geophys. Res.*, *106*(A1), 149–163.

Pätzold, M., S. Tellmann, B. Häusler, D. Hinson, R. Schaa, and G. L. Tyler (2005), A sporadic third layer in the ionosphere of Mars, *Science*, *310*, 837–839.

Pätzold, M., S. Tellmann, B. Häusler, D. Hinson, and G. L. Tyler (2006), A third layer in the ionosphere of Mars, paper presented at European Geosciences Union Meeting, Vienna, 3–7 Apr.

Picardi, G., et al. (2004), MARSIS: Mars Advanced Radar for Subsurface and Ionosphere Sounding, in *Mars Express: A European Mission to the Red Planet*, *Eur. Space Agency Spec. Publ. SP-1240*, 51–70.

Strangeway, R. J. (1996), Collisional joule dissipation in the ionosphere of Venus: The importance of electron heat conduction, *J. Geophys. Res.*, *101*(A2), 2279–2295.

M. H. Acuña, NASA Goddard Space Flight Center, Greenbelt, MD 20771, USA.

W. V. Boynton, Lunar and Planetary Laboratory, University of Arizona, Tucson, AZ 85721, USA.

D. A. Brain, Space Physics Research Group, Space Sciences Laboratory, University of California, Berkeley, CA 94720, USA.

D. A. Gurnett, R. L. Huff, D. L. Kirchner, and D. D. Morgan, Department of Physics and Astronomy, University of Iowa, Iowa City, IA 52242, USA. (david-morgan@uiowa.edu)

G. Picardi, Infocom Department, "La Sapienza," University of Rome, I-00184 Rome, Italy.

J. J. Plaut, Jet Propulsion Laboratory, Pasadena, CA 91109, USA.